6-1-2005

A Novel Hybrid Heat Sink using Phase Change Materials for Transient Thermal Management of Electronics

Shankar Krishnan

S V. Garimella
Purdue University, sureshg@purdue.edu

S. S. Kang

Krishnan, Shankar; Garimella, S V.; and Kang, S. S., "A Novel Hybrid Heat Sink using Phase Change Materials for Transient Thermal Management of Electronics" (2005). *CTRC Research Publications.* Paper 66.
http://dx.doi.org/10.1109/TCAPT.2005.848534

A NOVEL HYBRID HEAT SINK USING PHASE CHANGE MATERIALS FOR TRANSIENT THERMAL MANAGEMENT OF ELECTRONICS

Shankar Krishnan[1], **Suresh V. Garimella**[1] and **Sukhvinder S. Kang**[2]

[1]Cooling Technologies Research Center, School of Mechanical Engineering
Purdue University, West Lafayette, Indiana 47907 USA
Phone: (765) 494-5621, Fax: (765) 494-0539
Email: sureshg@ecn.purdue.edu

[2]Aavid Thermalloy, Concord, New Hampshire 03301 USA

ABSTRACT

A hybrid heat sink concept which combines passive and active cooling approaches is proposed. The hybrid heat sink is essentially a plate fin heat sink with the tip immersed in a phase change material (PCM). The exposed area of the fins dissipates heat during periods when high convective cooling is available. When the air cooling is reduced, the heat is absorbed by the PCM. The governing conservation equations are solved using a finite-volume method on orthogonal, rectangular grids. An enthalpy method is used for modeling the melting/re-solidification phenomena. Results from the analysis elucidate the thermal performance of these hybrid heat sinks. The improved performance of the hybrid heat sink compared to a finned heat sink (without a PCM) under identical conditions, is quantified.

In order to reduce the computational time and aid in preliminary design, a one-dimensional fin equation is formulated which accounts for the simultaneous convective heat transfer from the finned surface and melting of the phase change material at the tip. The influence of the location, amount, and type of PCM, as well as the fin thickness on the thermal performance of the hybrid heat sink is investigated. Simple guidelines are developed for preliminary design of these heat sinks.

Keywords: hybrid heat sinks, melting, phase change materials, transient power dissipation, electronics cooling

NOMENCLATURE

A	Area, m^2
Bi	Biot number (hL/k_f)
C_p	Isobaric specific heat capacity, J/kgK
D_h	Hydraulic diameter, m
f_l	Fraction of liquid
H	Height of the heat sink, m
h	Heat transfer coefficient, W/m^2K
k	Thermal conductivity, W/mK
L_{exp}	Exposed length of the fin, m
L_{pcm}	Length of the fin immersed in PCM, m
L	Total length of the fin, m
P	Perimeter, m
Q	Heat transfer rate, W
S	Half-spacing between the fins, m
Ste	Stefan number ($C_p\Delta T/\Delta H$)
t	Time, s
T	Temperature, K

Greek symbols

α	Thermal diffusivity, m^2/s
β	Coefficient of thermal expansion, K
δ	Melt depth, m
ΔH	Latent heat of melting/fusion, kJ/kg
ε	Mushy zone thickness, °C
ϕ	Percentage increase in heat transfer rate, %
ρ	Density, kg/m^3

Subscripts

b	Base
c	Cross-sectional
f	Fin
max	Maximum

melt Melting temperature

min Minimum

o Initial, Overall

pcm Phase change material

t Total

∞ Ambient

INTRODUCTION

Phase change materials have traditionally been used in low-temperature thermal energy storage for residential heating and industrial heat exchanger units [1,2,3], and in aerospace applications [4]. More recently, phase change materials (PCMs) have been explored for electronics thermal management. Applications considered have included handsets, portables, and power electronics [5,6,7,8,9]. These materials are particularly attractive for transient applications where the heat loads are pulsed [10,11]. Commonly used PCMs (e.g., paraffin) have very low thermal diffusivity and are not particularly suitable for transient applications. In order to improve the effective thermal conductivity and enhance heat transfer rates, internal fins and metal foams have been introduced into the PCM [12,13,14,15].

A number of electronics thermal management applications encounter time-dependent cooling conditions such that the cooling rate periodically changes between high and low values. Energy-efficient thermal management solutions [16,17], which feature periodic on/off cycles for the fan/blower, also fall under this category. Other transient or limited-duty-cycle situations occur in power surges, back-up cooling units, and temporary fan-failure scenarios.

In the present study, a hybrid heat sink concept targeted towards these applications is proposed. The heat sink consists of a parallel-plate heat sink with a portion of the fin tips immersed in a suitable phase change material. The heat sink concept is first explained below, followed by an analysis methodology. A fin equation which accounts for simultaneous convective heat transfer from the fin and melting of the PCM at the tip is then developed. The influence of PCM type, location and amount, as well as the fin thickness, on the thermal performance of the system is investigated. Simplified design guidelines are also formulated for preliminary design of these heat sinks, and the merits of the proposed hybrid heat sink concept discussed.

NOVEL HEAT SINK CONCEPT

Finned heat sinks are widely used to cool electronics. In a number of applications, the velocity fluctuates periodically from a high value to a low value, with a corresponding time-dependence in the heat transfer coefficient at the fin surface. In the proposed hybrid heat sink concept (Figure 1), the fins dissipate heat through their exposed area during periods of high convective air cooling (h_{high}). The PCM at the fin tips participates by absorbing heat when the convective cooling rate is reduced (h_{low}). The heat stored in the PCM is rejected to the ambient (re-solidification) during the subsequent jump in convection in the next cycle.

If the entire finned structure were completely immersed in a PCM, the heat sink would initially perform better than the proposed arrangement. However, as the heat source continually dissipates heat, such a design would not sustain its dissipation capability since the melted PCM would become superheated. The advantage of the proposed concept is that it can dissipate heat continuously as the melted PCM re-solidifies during periods of high convective cooling. The thermal performance of these hybrid heat sinks can be optimized by proper choice of the governing parameters.

MATHEMATICAL AND NUMERICAL MODELING

The problem domain considered for the analysis of the proposed heat sink is shown in Figure 2. Symmetry conditions simplify the domain to include half the thickness of a fin and half the PCM volume between two fins. The fin base is maintained at a constant temperature, T_b (= 85°C). As a worst case, the plane at the right is assumed adiabatic. The exposed part of the fin and the PCM exchange heat transfer with the ambient (at T_∞ = 35°C) that imposes a time-dependent convective heat transfer coefficient, h. Heat transfer coefficients of 20 W/m^{2}K and 125 W/m^{2}K were used as the low and high values (Figure 1) for all numerical calculations. The spacing between the fins is 2S, and the fin thickness, t_f. Thermophysical properties of the fin material (aluminum) and the PCMs considered are listed in Table 1 [12,18,19,20]. The governing energy conservation equation may be written as:

$$\rho\left(C_p + \Delta \mathrm{H} \ \frac{\partial f_l}{\partial T} \right) \frac{\partial T}{\partial t} = \vec{\nabla}.\left(k \vec{\nabla} T \right) \qquad (1)$$

The effective (or apparent) heat capacity method is used to model the phase change problem. Details of the mathematical model can be obtained from [21].

The computational domain is discretized into orthogonal finite volumes. A central differencing scheme is used for approximating the spatial fluxes and a three-time-levels scheme is implemented for temporal terms [22]. Since numerical methods have difficulty in handling step-functions, the fraction of liquid is smoothed [23] according to:

$$f_l = \begin{cases} 0 & T_p < \left(T_{melt} - \varepsilon\right) \\ \dfrac{T_p - T_{melt} + \varepsilon}{2\varepsilon} & \left(T_{melt} - \varepsilon\right) \le T_p \le \left(T_{melt} + \varepsilon\right) \\ 1 & T_p > \left(T_{melt} + \varepsilon\right) \end{cases}$$

Numerical solutions of the energy equations are insensitive to the assumed variation of f_l with temperature if ε is small. For the computations performed in this study ε was maintained at 0.1°C. Iterations were terminated when the residuals [22] dropped below 1×10^{-4}. Grid-independence of the numerical solution was tested using three increasingly fine grids (52×24, 101×47 and 152×69). The intermediate mesh (101×47) was found to be sufficient for all the calculations presented in this study. The numerical code used for the present calculations has previously been validated against benchmark experimental and numerical results extensively [21, 24]. Further details about the numerical procedure and benchmark solutions can be obtained from [21, 24].

RESULTS AND DISCUSSION

Results for a representative case are first considered in detail. The total length of the fin is 100 mm, of which 30 mm is immersed in the PCM. The fin thickness and spacing are 1 mm and 7.5 mm, respectively. An ambient heat transfer coefficient (h_{low}) of 20 W/m^{2}K was maintained for the first 600 s, and then increased (h_{high}) to 125 W/m^{2}K, allowing the PCM to re-solidify.

Solid/liquid front locations at various times are plotted in Figure 3 for the PCM, Suntech P116. The entire domain was initially at the ambient temperature (35°C). The upper half of the plot shows the temporal evolution of the melt front while the lower half shows the re-solidifying front. The PCM took approximately 1650 s to re-solidify completely and hence the total cycle (melting and re-solidification) time was 2250 s.

Due to the lower thermal conductivity of the PCM compared to the fin, the heat penetrates deep into the fin first, before spreading into the PCM and melting it. This results in the front shape being approximately parallel to the horizontal axis. Indeed, for infinite fin thermal conductivity, the melt shape would be truly parallel to the x-axis, and the melting one-dimensional in nature. The curvature in the melt fronts at the left wall is due to convective heat losses. For a melting process completely dominated by conduction heat transfer (with initial PCM temperature being at T_{melt}), the melt depth scales as [25]

$$\delta \sim \sqrt{Ste(x)\left(\alpha_{pcm} t\right)} \tag{2}$$

where $Ste(x) = C_p[T_f(x) - T_{melt}]/\Delta H$. This expression is useful in the discussion of heat sink design guidelines to be presented later in this paper. In order to use equation (2) without any additional calculations, the fin temperature $T_f(x)$ must be known. This can be approximated as the temperature of the fin (with an adiabatic tip) if the entire fin were exposed to the ambient ($h = 20$ W/m^{2}K and $T_\infty = 35$°C). The actual temperature of the fin would be less than this approximation suggests, as seen in Figure 4). Using equation (2) for times of 200 s and 600 s at $x = 71$ mm, the melt depths obtained are 1.7 mm and 2.9 mm, respectively. The corresponding melt depths obtained from CFD calculations at $x = 71$ mm are 1.35 and 2.8 mm, respectively. At 600s, the average melt front location was at 2.4 mm, with only 64% of the domain having melted. In Figure 4, the temporal evolution of the fin temperature distribution is plotted for Suntech P116. Also plotted in Figure 4 are the steady-state temperature distributions for the case when the entire fin was exposed to ambient air with the tip being adiabatic, both for the low (20 W/m^{2}K) and high (125 W/m^{2}K) convection ambient; as expected, these provide upper and lower temperature bounds in the figure. It may be noted that the fin temperatures are suppressed for the hybrid heat sink compared to the fin exposed only to low-convection ambient.

Front locations during re-solidification, shown in the lower half of Figure 3, show that the solid begins to grow from the left end and from the fin surface. The heat flow into the fin at the base is countered by heat added due to the resolidification of the PCM, resulting in the reversal in heat flow direction into the fin evident in Figure 4. The front shape in Figure 3 results from heat being lost directly to the ambient as well as through the fin.

The re-solidification process is schematically explained in Figure 5. Along the plane AD, heat is lost directly to the ambient which is at 35 °C with $h = 125$ W/m^{2}K. Heat is lost to the ambient through the fin along plane AB. Region AEFG in Figure 5 clearly experiences two-dimensional

heat flow due to the interaction between both these heat loss paths. Ignoring region AEFG, the problem may be simplified into a two one-dimensional sub-problems, one governed by heat loss across plane GD and the other across plane EB. The solidification times for these two 1D sub-problems are given, respectively, by the following expressions, in which *w* and *d* are marked in Figure 5 [26]:

$$t_{solidify} \approx \frac{w^2 \rho \Delta H}{2k_{pcm}\left(T_{melt} - T_{\infty}\right)}\left(1 + \frac{2k_{pcm}}{h_{high} w}\right) \tag{3}$$

$$t_{solidify} \approx \frac{d^2}{\alpha_{pcm}} \frac{1}{Ste(x)} \tag{4}$$

In equation (4), Stefan number is defined as $C_p(T_{melt} - T_f(x))/\Delta H$. These equations were derived [26] by assuming the process to occur under quasi-steady conditions, with initial temperature being the melting temperature. The fin temperature distribution can be assumed to be the same as the fin temperature when the entire fin is exposed to air. At 1650 s, the predicted value for *w* (Figure 5) from Equation (3) is 4.9 mm. At the location x = 75 mm and t = 1650 s, the predicted melt depth, *d*, from equation (4) is 3.8 mm. These approximate values of *w* and *d* compare with the predicted values (Figure 3) of 5.1 and 2.5 mm, respectively.

In Figure 6, the temporal evolution of the melting and re-solidifying front locations is plotted for a Bi/Pb/Sn/Cd/In eutectic alloy (melting point of 47°C, same as for Suntech P116). This metallic alloy is chosen for comparative simulation in spite of the presence of lead and cadmium since it has the same melting point as that of Suntech P116, but a diffusivity that is two orders of magnitude higher. Other low-melting alloys could be chosen in practice. The upper half of Figure 6 shows the melting front locations at various times, while the lower half shows the solidifying fronts. The fin length, thickness and spacing are same as in the previous case as are the transient convective conditions. The domain was again initially at an ambient temperature of 35°C. The effect of the higher diffusivity of the alloy can be seen clearly by comparing Figure 6 with Figure 3. The time for heat to penetrate into the domain scales as L_c^2/α, where L_c is the characteristic length: L_c for the PCM is S and for the fin is L_{pcm}. Since $S^2/\alpha_{pcm} << L_{pcm}^2/\alpha$, the front for the metallic alloy (Figure 6) is very steep compared to paraffin in Figure 3. The metallic alloy took approximately 575 s to melt completely. The ratio of the available latent heat ($\rho\Delta H$) of the metallic alloy to that of the paraffin is ≈ 0.6. For identical boundary and initial conditions and PCM melting points, neglecting the initial sub-cooling, the

ratio of amounts of melted alloy to paraffin is the inverse of their available latent heat energy, i.e.:

$$\frac{(\Delta V)_{paraffin}}{(\Delta V)_{metallic\,alloy}} \approx \frac{(\rho \Delta \mathrm{H})_{metallic\,alloy}}{(\rho \Delta \mathrm{H})_{paraffin}} \tag{5}$$

The approximate Equation (5) yields a value of 0.6 at end of 600 s, which agrees well with the "exact" value of 0.64 from the numerical prediction.

After 600 s, the ambient heat transfer coefficient was increased to 125 W/m^{2}K and the completely melted alloy started to solidify; complete solidification took 1250 s, for a total phase change cycle time of 1850 s. The temperature distributions in the fin are plotted in Figure 7 for various times with the PCM; steady-state distributions for the low- and high-convection ambient conditions are also plotted. Comparing Figure 7 with Figure 4, the temperatures in the fin are seen to be lower for the alloy than for the paraffin.

The temperature distributions for the two PCM materials of very different thermal diffusivities (Suntech and metallic alloy) are compared in Figure 8; profiles along the y-coordinate at x = 75 mm are shown at different times. During the heat-input period (up to 600 s), the Suntech PCM is still undergoing phase change as indicated by the temperature gradient in the melt. In contrast, the metallic alloy has already melted and the molten liquid continues to pick up sensible heat during this time. Complementary trends may be noted during the cooling period (profiles at t = 1500 s shown in the figure), where the paraffin is still undergoing phase change while the metallic alloy has already solidified.

In Figure 9, the fin heat transfer rates for both paraffin and metallic alloy are shown. Also included in this figure is the case where the entire length of the fin is exposed to air, and no PCM is used. For the first 600 s, with the heat transfer coefficient at 20 W/m^{2}K, the fins with the PCM performed better than those without PCM. During this period, the fin heat transfer rate drops as time evolves because more PCM melts. Figure 9 also shows a steep decrease in the heat transfer rate initially due to the sensible heating of the PCM from the initial temperature to the melting point of the PCM (35 to 47°C). After 9 mins, the fin immersed in metallic alloy is able to dissipate 6 W (~ 14 %) more than the baseline case of no PCM; the paraffin was similarly able to dissipate 4.2 W (~ 10 %) more than the baseline case. During resolidification in contrast, although the fins with PCMs dissipate less heat than the fin without PCM (due to the resistance to heat flow posed by the PCM), the difference is not as pronounced as during the melting

period. Moreover this difference diminishes as the solid grows and the heat transfer rate with the PCM increases. The percentage of overall improvement (ϕ) in the heat transfer rate for the fins immersed in a PCM over the fins without PCM, given by $\left(1-\frac{Q_{\text{no PCM}}}{Q_{\text{with PCM}}}\right)\times 100$, is plotted in Figure 10.

Influence of Natural Convection in the PCM Melt

The effect of natural convection in the melt was also simulated, to verify whether the conduction-only solutions above are reasonable. Details of the simulation of natural convection are provided in [21, 24]. Due to the chosen heat sink orientation, the symmetry condition imposed on the top end of the domain in Figure 2 (at $y = S + t_f/2$) is no longer valid, and was relaxed and the PCM in the entire inter-fin spacing was simulated as shown in Figure 11. The viscosity and thermal expansion coefficient for the Suntech PCM were not available and properties for a similar paraffin, eicosane, were used instead – thus, although the exact magnitudes of velocities would be somewhat different, the effect of natural convection can still be explored. The front locations with and without including natural convection in the melt at two different times are shown in Figure 12. It is clear that the natural convection in the melt is not pronounced in this case, and the heat transfer process is conduction-dominated. It may be noted that a Rayleigh number defined for this situation would vary with time as the melt front, and hence the height of the liquid column, evolves.

DESIGN METHODOLOGY

Quasi-Steady Model

An easy-to-use quasi-steady model for the heat transfer through the fin (shown in Figure 2) is now derived. This model simplifies the analysis of the proposed hybrid heat sink and aids in its preliminary design. The following assumptions are invoked in the present model:

- Heat transfer in the fin is one-dimensional (thin fin approximation) along the x-direction.
- The heat transfer process is quasi-steady.
- Melting is also one-dimensional (along the y-direction).
- The PCM is initially at melting temperature.
- The heat transfer from the PCM to the ambient is not included; the PCM only communicates with the fin.

Accounting for the convective heat transfer and melting of the PCM from the fin surface, the governing energy conservation equation for the fin can be written as

$$k_f A_c \frac{d^2T}{dx^2} - hP\left(T - T_\infty\right) + hP\left(T - T_\infty\right)\left[u\left(x - L_{\exp}\right)\right] - k_{pcm} P \frac{\left(T - T_{melt}\right)}{\delta}\left[u\left(x - L_{\exp}\right)\right] = 0 \tag{6}$$

in which δ is the melt depth and is defined as

$$\delta = \sqrt{\frac{2k_{pcm}}{\rho \Delta H}\int_{t_0}^{t}\left(T - T_{melt}\right)dt} \tag{7}$$

In equation (6), $u(x - L_{exp})$ is a unit step function (Heaviside function) defined as

$$u\left(x - L_{\exp}\right) = \begin{cases} 0, & if \quad x < L_{\exp} \\ 1, & if \quad x > L_{\exp} \end{cases} \tag{8}$$

The quasi-steady approximation yields accurate results when the initial temperature of the domain is equal to the melting point or when the Stefan number is small (Ste $\rightarrow$ 0) [26]. Equation (6) is similar to the one reported by Sasaguchi and Kusano [27] for the solidification of water from a finned surface completely immersed in a water-saturated porous medium.

Upon non-dimensionalizing Equation (6) using $(T_b - T_\infty)$ and L as the temperature and length scales, respectively, the heat sinking terms (convective and phase change) can be compared to indicate whether the hybrid heat sink will perform better than a conventional heat sink without PCM. This condition can be expressed with the Biot number defined as $h_{low}L/k_f$ as:

$$Bi < \frac{k_{pcm}}{k_f}\frac{L_{pcm}}{\delta} \tag{9}$$

If this inequality is satisfied, then the hybrid heat sink performs better than the conventional design.

Parametric Analysis

The effects of key governing parameters in the hybrid heat sink design are highlighted next. From Equation (6), the important parameters affecting the heat transfer process are seen to be the amount of PCM (L_{pcm}), fin thickness ($t_f \sim A_c/P$), thermal conductivity ratio (k_{pcm}/k_f) and the PCM melting point (T_{melt}). The total length of the fin is 100 mm with a fin thickness of 1 mm as before. The base temperature is 85°C, and the heat transfer coefficient and ambient temperature are 20 W/m^{2}K and 35°C, respectively. In the derivation of Equation (6) since initial

temperature of the PCM is assumed to be its melting point for simplification, eicosane with a melting point of 36°C is chosen as the PCM in this analysis. This simplified model is not valid PCMs of high thermal diffusivity, in which the phase change process would be necessarily two-dimensional. For eicosane, on the other hand, good correspondence is seen between predictions from CFD and from Equation (6): for instance, at 300 s, the fin heat transfer rate predicted by the two methods is 43.5 W and 42.3 W, respectively.

The influence of amount of PCM coverage on the temperature distribution in the fin is plotted in Figure 13. As the amount of PCM increases, the performance of the heat sink improves in terms of lowering the fin temperature, and equivalently, increasing the heat flow rate supported. Figure 14 shows the melt depth calculated at the end of 600 s for L_{pcm} = 50 mm and 100 mm. For the case when the entire length of the fin is immersed in PCM, the melt depth is high as the PCM is proximal to the heat source.

The effect of varying the fin thickness on the melt depth is shown in Figure 15. For fixed base temperature and ambient conditions, an increase in fin thickness (and thus in cross-sectional area) increases the fin heat flow rate at the base. This increase in heat flow rate increases the temperature in the fin, and leads to greater melting in the PCM. The fin heat transfer rate for fixed base temperature at the end of 600 s for 0.5, 1 and 2 mm-thick fins is 31.4, 41.9 and 50.6 W, respectively.

Figure 16 shows the melt depth for three different PCMs. At the end of 600 s, the melt depths in eicosane and heneicosane are almost equal. Although the melting point of heneicosane is approximately 4°C higher, this is balanced in terms of melt depth by the available latent heat energy ($\rho\Delta H$) for eicosane being 14% higher. On the other hand, the latent heat energy for Suntech is comparable to that of eicosane, but its higher melting point leads to slower melting.

Design Guidelines

For a specified heat sink volume, ambient temperature, allowable maximum temperature and pressure drop through the heat sink (which sets the convective condition), an optimum hybrid heat sink may now be designed for maximum heat transfer rate. The first step in designing the hybrid heat sink is to obtain a thermally optimized baseline heat sink (without PCM) using well-known optimization techniques [28]. The next step is to select the appropriate PCM for the application. In order to determine the required PCM melting temperature, a rough estimate of the fin length to be immersed in the PCM is needed. Using equation (9),

$$L_{pcm} > \left(\frac{h_{low} L}{k_{pcm}} \right) S$$

where S is the half-spacing between the fins already determined in the first step. The thermal conductivity k_{pcm} also needs to be selected: for low heat sink mass, organic PCMs are suitable, but their thermal conductivities are of O(0.2); if mass is not a concern, then low-melting solders with conductivities of O(15) are preferred. This expression only sets the minimum length required. The maximum value of L_{pcm} is set by the selected PCM melting point. The melting point is constrained by the ambient temperature, $T_{melt} > T_\infty$, to allow for re-solidification. A second constraint on the melting point is imposed by the fin temperature at $x = L_{exp}$ for the case when the entire fin is exposed to air at h_{low}. Using the steady-state temperature distribution for a fin with an adiabatic tip exposed to a constant h_{low}, this condition becomes:

$$\left(T_{melt}\right)_{\max} = T_\infty + \left(T_b - T_\infty\right) \frac{\cosh\left(m_{low} L_{pcm}\right)}{\cosh\left(m_{low} L\right)} > T_{melt} \tag{10}$$

where $m_{low} = \sqrt{h_{low} P / k A_c}$. In fact this is the maximum melting temperature of the PCM that can be used as higher temperatures would degrade the performance of the hybrid heat sink below that of the baseline heat sink.

A third constraint on the PCM selection is imposed by the requirement for re-solidification of the melted PCM. For h_{high}, the temperature at $x = L_{exp}$ imposes a minimum on the melting temperature that can be expressed as

$$\left(T_{melt}\right)_{\min} = T_\infty + \left(T_b - T_\infty\right) \frac{\cosh\left(m_{high} L_{pcm}\right)}{\cosh\left(m_{high} L\right)} < T_{melt} \tag{11}$$

in which $m_{high} = \sqrt{h_{high} P / k A_c}$; for very high heat transfer coefficients, $(T_{melt})_{min} = T_\infty$. Equations (10) and (11) specify the maximum and minimum allowable melting points, from which a suitable PCM can be chosen. The periods of transient operation of the hybrid heat sink can be found from Equations (2), (3) and (4) discussed earlier. These simplified equations do not apply when the PCM has a thermal diffusivity comparable to that of the fin material, as in the case of metallic alloys.

CONCLUSIONS

A hybrid heat sink concept, combining a plate fin heat sink with immersion into a phase change material, is proposed. A rigorous computational analysis, including the effects of natural convection in the melt, was performed, and compared to more simplified analyses. The ability of the heat sink to operate continuously under time-varying cooling conditions is investigated. Easy-to-use design guidelines are developed for the hybrid heat sink, in terms of geometry and material properties.

Different phase change materials (organic and metallic) were evaluated. The metallic PCM performed better than the organic PCM owing to its superior thermal diffusivity. The high density of the metallic PCM, on the other hand, may render it an unsuitable choice for low-weight heat sink designs. The fin heat transfer rate increased with an increase in fin thickness and amount of PCM and decreasing melting temperature of the PCMs.

Acknowledgements

Support for this work from industry members of the Cooling Technologies Research Center, an NSF Industry/University Cooperative Research Center (www.ecn.purdue.edu/CTRC), is gratefully acknowledged. Helpful suggestions on the numerical model from Professor Jayathi Murthy of Purdue University are appreciated.

REFERENCES

[1] J. Eftekhar, A. Haji-Sheikh and D. Y. S. Lou, "Heat Transfer Enhancement in a Paraffin Wax Thermal Storage System," *Journal of Solar Energy Engineering*, vol. 106, pp. 298 – 306, 1984.

[2] N. Shamsundar and R. Srinivasan, "Effective-NTU Charts for Heat recovery from Latent Heat Storage Units," *Journal of Solar Energy Engineering*, vol. 102, pp. 263 – 271, 1980.

[3] S. M. Hasnain, "Review of Sustainable Thermal Storage Technologies, Part I: Heat Storage Materials and Techniques," *Energy Conversion Management*, vol. 39, pp. 1127 – 1138, 1998.

[4] W. R. Humphries and E. L. Griggs, "A Design Handbook of Phase Change Thermal Energy Storage Devices," NASA TP 1074, 1974.
[5] C. Jing, V. Martin and F. Setterwall, "The Study of PCM Thermal Management Solution for Portable Computer," *IEA ECES IA Annex 17, Advanced Thermal Energy Storage Techniques, 2nd Workshop*, 3-5 Apr. 2002, Ljubljana, Slovenia.
[6] N. Leoni and C. H. Amon, "Thermal design for transient operation of the TIA wearable portable computer," *Advances in Electronics Packaging*, pp. 2151 – 2161, 1997.
[7] E. M. Alawadhi and C. H. Amon, "Thermal analyses of a PCM Thermal Control Unit for Portable Electronic Devices: Experimental and Numerical Studies," *IEEE CPMT*, Vol. 26, pp. 116 – 125, 2003.
[8] M. Hodes, R. D., Weinstein, S. J. Pence, J. M. Piccini, L. Mouzione and C. Chen, "Transient Thermal Management of a Handset using Phase Change Material (PCM)," *ASME Journal of Electronic Packaging*, vol. 124, pp. 419 – 426, 2002.
[9] A. G. Evans, M. Y. He, J. W. Hutchinson and M. Shaw, "Temperature Distribution in Advanced Power Electronics Systems and the effect of Phase Change Materials on Temperature Suppression during Power Pulses," *ASME Journal of Electronic Packaging*, vol. 123, pp. 211 – 217, 2001.
[10] E. M. Alawadhi and C. H. Amon, "Performance Analysis of an Enhanced PCM Thermal Control Unit," *Procs. ITHERM 02*, pp. 283 – 289, 2000.
[11] S. Krishnan and S. V. Garimella, "Performance Analysis of a Phase Change Energy Storage System for Pulsed Power Dissipation," *Procs. ITHERM 02*, pp. 476 – 484, 2002.
[12] J. Leland and G. Recktenwald, "Optimization of a Phase Change Heat Sink for Extreme Environments," *SEMITHERM03*, pp. 351- 356, 2003.
[13] V. Shatikian, V. Dubovsky, G. Ziskind and R. Letan, "Simulation of PCM Melting and Solidification in a Partitioned Storage Unit ," *Procs. ASME Summer Heat Transfer Conference*, HT2003-47167, 2003.
[14] S. Krishnan, J. Y. Murthy and S. V. Garimella, "A Two-Temperature Model for the Analysis of Passive Thermal Control Systems for Electronics," *ASME Journal of Heat Transfer*, Vol. 126, pp. 628 – 637, 2004.
[15] S. Krishnan, J. Y. Murthy and S. V. Garimella, "A Two-Temperature Model for Solid/Liquid Phase Change in Metal Foams," *ASME National Heat Transfer Conference*, Charlotte, North Carolina, HT-FED-56337, 2004.
[16] M. Iyengar and A. Bar Cohen, "Least-Energy Optimization of Forced Convection Plate-Fin Heat Sinks," *IEEE CPMT*, vol. 26, pp. 61-70, 2003.
[17] D. Yoo and Y. Joshi, "Energy Efficient Thermal Management of Electronic Components using Solid Liquid Phase Change Materials," *Procs. ITHERM 02*, pp. 800 – 807, 2002.
[18] S. Himran, A. Suwono and G. A. Mansoori, "Characterization of Alkanes and Paraffin Waxes for Application as Phase Change Energy Storage Medium," *Energy Sources*, vol. 16, pp. 117-128, 1994.
[19] F. P. Incropera and D. P. DeWitt, *Fundamentals of Heat and Mass Transfer*. John Wiley & Sons: New York, 1998.
[20] Alloy Digest, Engineering Alloy Digest Inc., New Jersey.
[21] J. E. Simpson, S. V. Garimella, and H. de Groh III, "An Experimental and Numerical Investigation of the Bridgman Growth of Succinonitrile," *AIAA Journal of Thermophysics and Heat Transfer*, vol. 16, pp. 324 - 335, 2002.

[22] J. H. Ferziger and M. Peric, *Computational Methods for Fluid Dynamics*. Springer-Verlag: Berlin, 1996.
[23] Dantzig, J. A., "Modeling Liquid-Solid Phase Changes with Melt Convection," *International Journal of Numerical Methods in Engineering*, vol. 28, pp. 1769-1785, 1989.
[24] S. Krishnan, "Analysis of Phase Change Energy Storage Systems for Pulsed Power Dissipation," M.S.M.E. Thesis, Purdue University, 2002.
[25] P. Jany and A. Bejan, "Scaling Theory of Melting with Natural Convection in an Enclosure," *International Journal of Heat and Mass Transfer*, vol. 31, pp. 1221 – 1235, 1988.
[26] V. Alexiades and A. D. Solomon, *Mathematical Modeling of Melting and Freezing Processes*. Hemisphere: Washington, 1993.
[27] K. Sasaguchi and K. Kusano, "Solid/Liquid Phase Change Heat Transfer in Porous Media (Effects of Fins on the Solidification Process)," *Heat Transfer – Japanese Research*, vol. 22, pp. 398 – 415, 1993.
[28] D. Liu and S. V. Garimella, "Analysis and Optimization of the Thermal Performance of Microchannel Heat Sinks," *InterPACK'03*, ASME Paper No. 35260, 2003.

List of Tables

List of Figures

List of Tables:

Table 1: Thermophysical properties of the materials used [12,18,19,20].

	ρ kg/m^3	k W/mK	ΔH kJ/kg	T_{melt} °C	C_p J/kgK
Eicosane	785	0.15	247	36	2460
Heneicosane	788	0.15	213	40.4	-
Suntech P116	818	0.24	266.0	47	2730
Bi/Pb/Sn/Cd/In	9160	15.0	14.0	47	147
Aluminum	2700	200	-	-	903

List of Figures

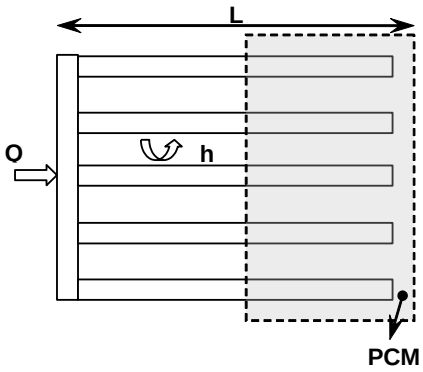

Figure 1: The proposed hybrid heat sink concept.

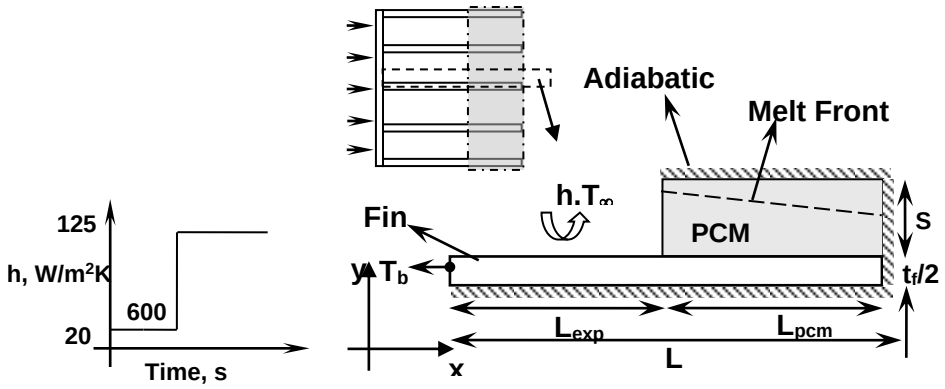

Figure 2: Schematic of the problem domain.

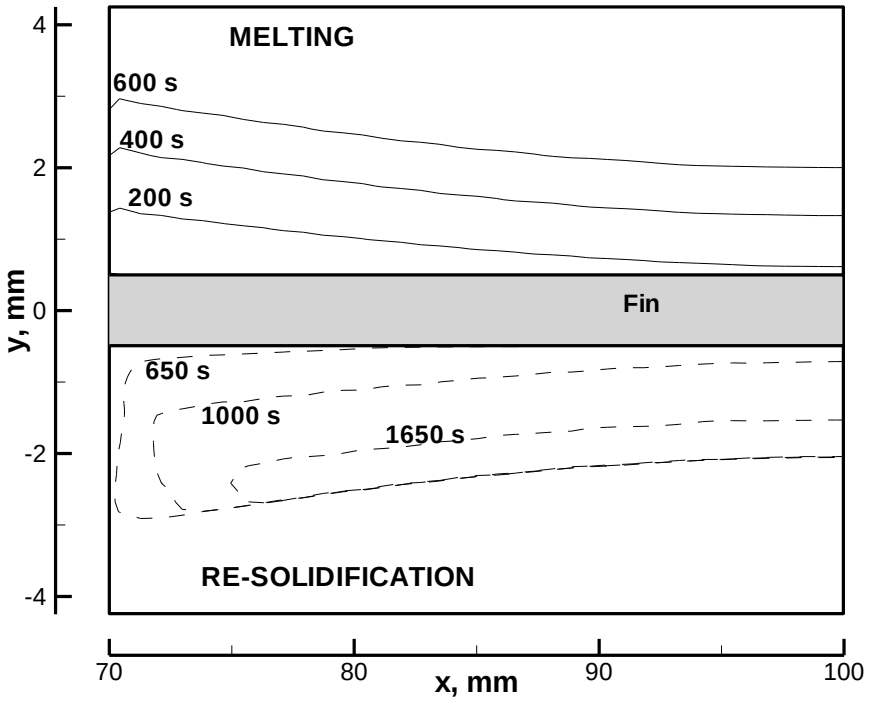

Figure 3: Temporal evolution of melting (top half) and re-solidifying (bottom half) front locations for Suntech P116.

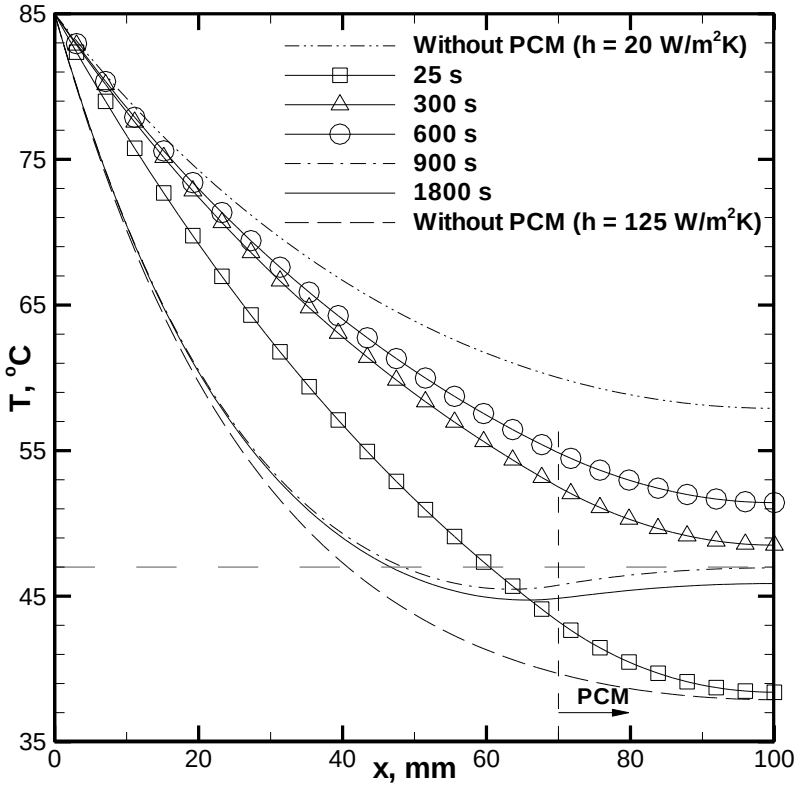

Figure 4: Fin temperature distribution at various times for Suntech P116; melting ends and resolidification starts at 600 s. The horizontal dashed line shows the melting point of the PCM.

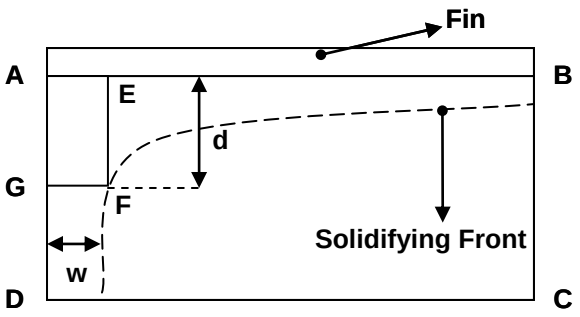

Figure 5: Schematic representation of the re-solidification process.

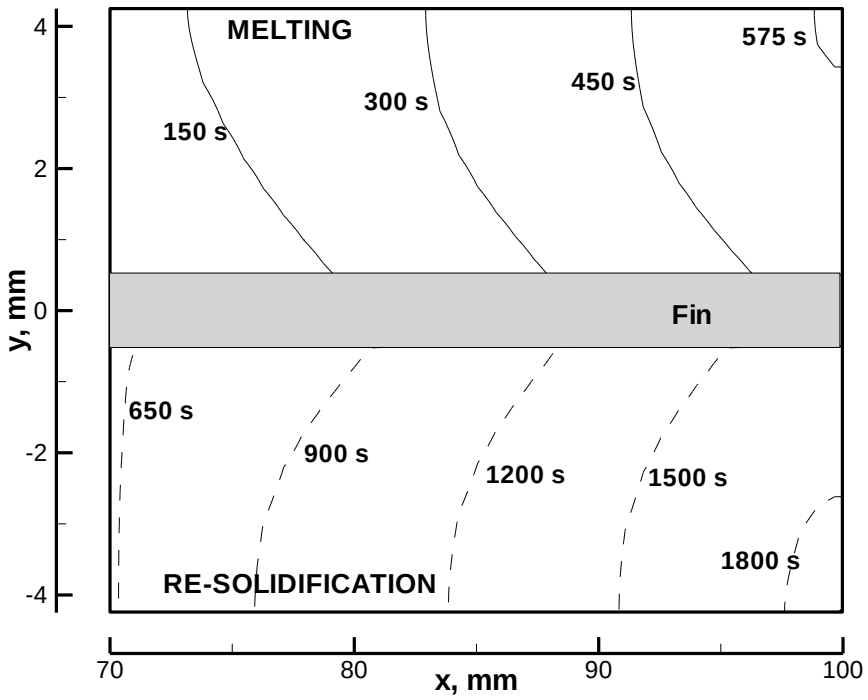

Figure 6: Temporal evolution of melting (top half) and re-solidifying (bottom half) front locations for metallic alloy.

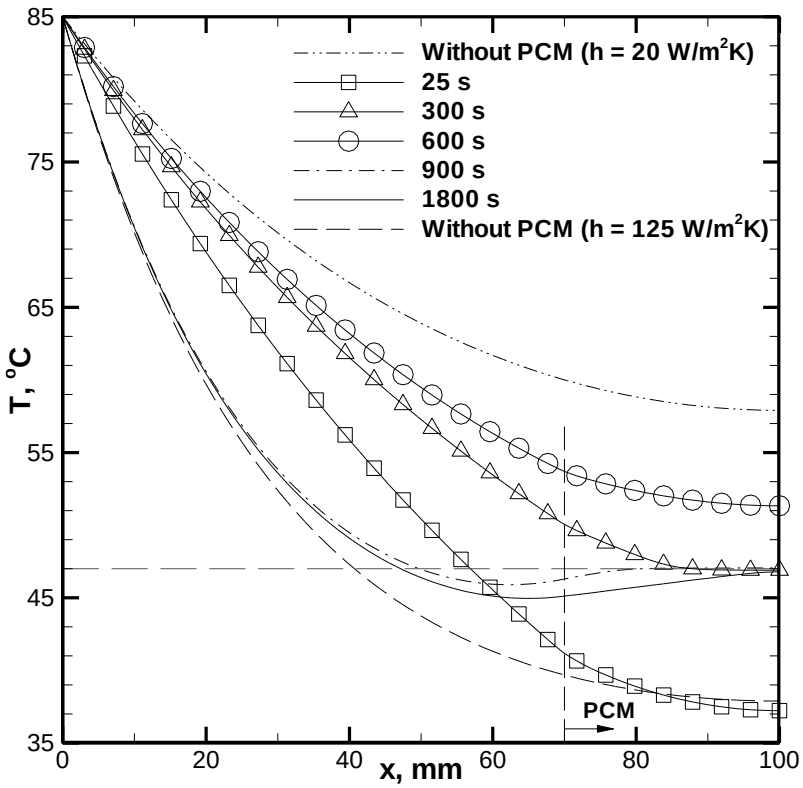

Figure 7: Fin temperature distribution at various times for the metallic alloy; melting ends and resolidification starts at 600 s. The horizontal dashed line shows the melting point of the PCM.

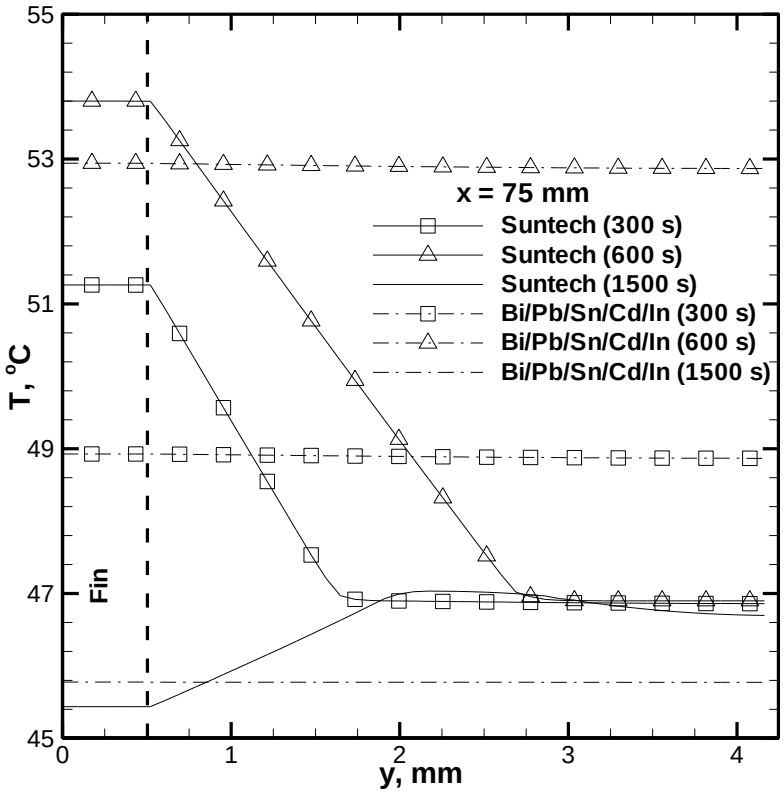

Figure 8: Temperature distribution in the y-direction at x = 75 mm for the two PCMs at different times; lines with symbols indicate the melting period and those without symbols indicate the re-solidification period).

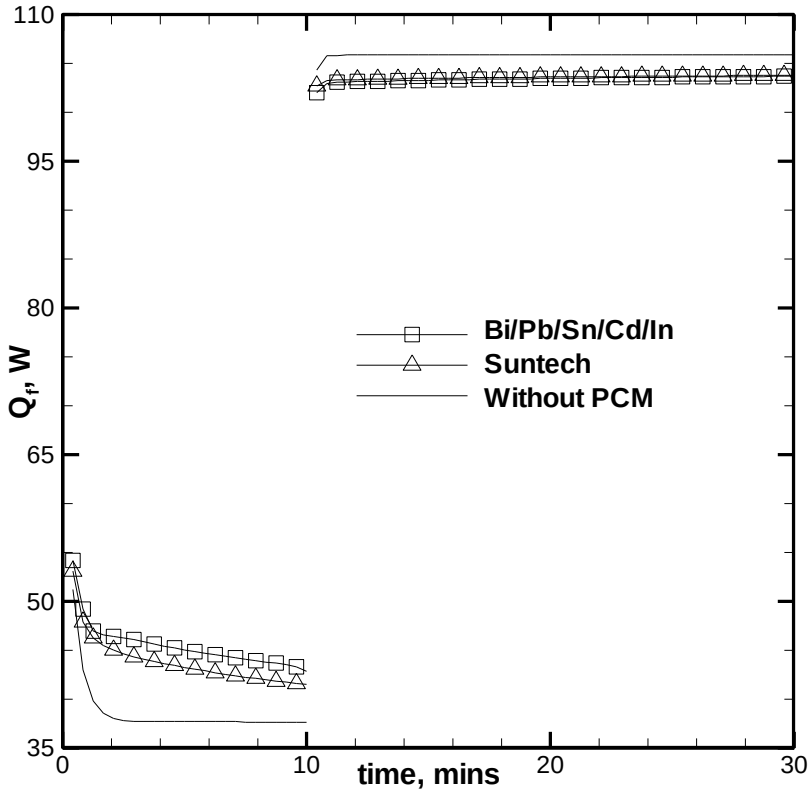

Figure 9: Fin heat transfer rate as a function of time.

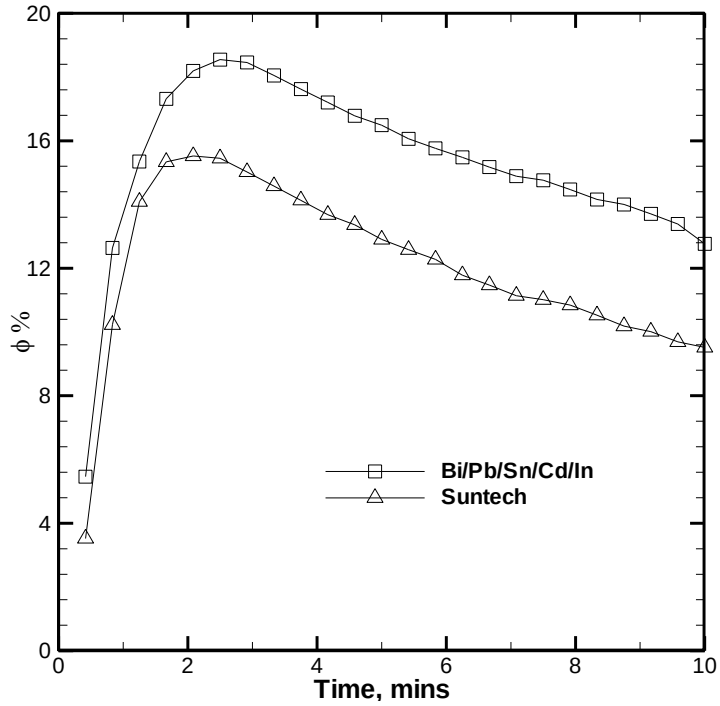

Figure 10: Percentage improvement in the heat transfer rate for the fins with PCM over the fins without PCM.

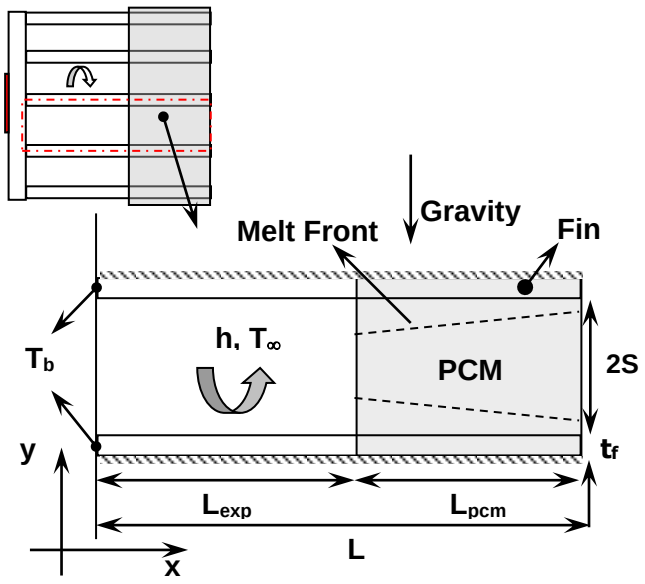

Figure 11: Schematic of the problem domain for simulating natural convection in the melt; the symmetry exploited earlier in Figure 3 is no longer valid when convection is included.

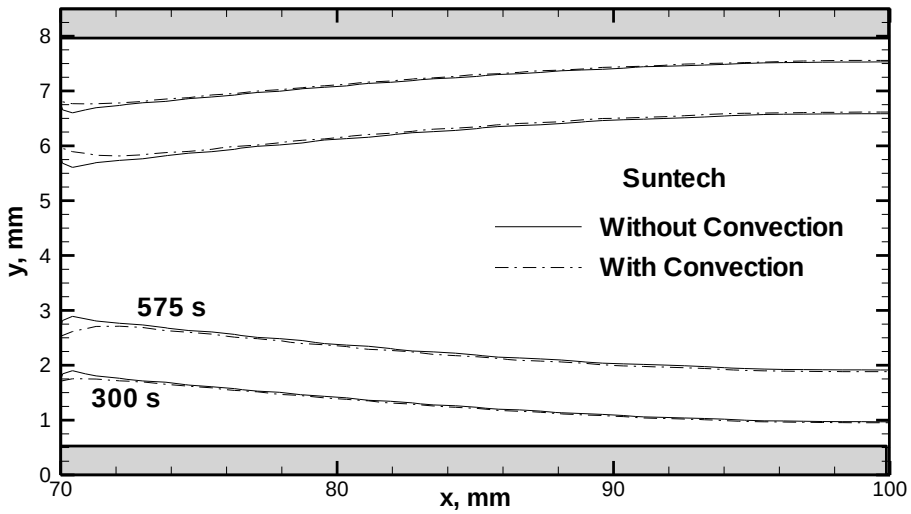

Figure 12: Melt front locations at two different times for Suntech PCM with and without natural convection in the melt.

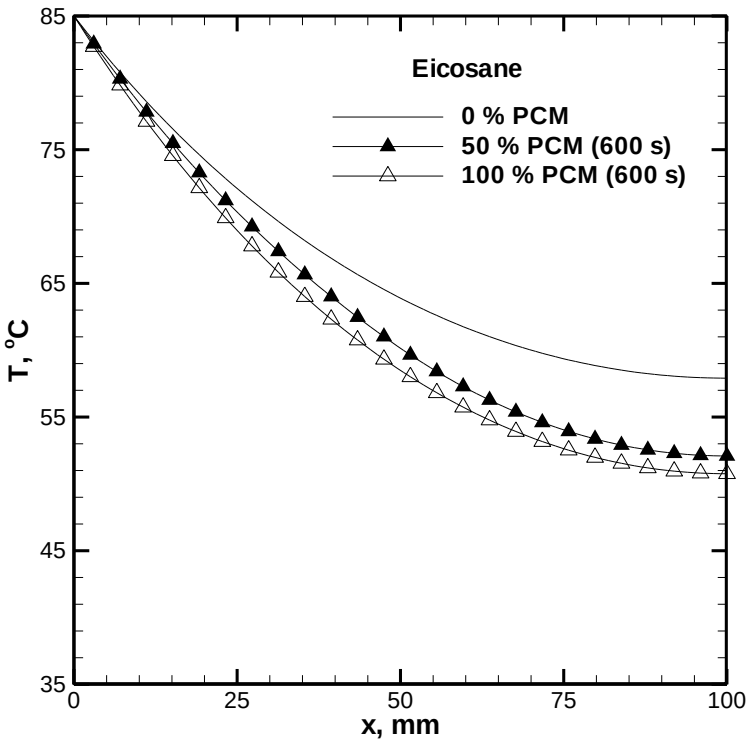

Figure 13: Temperature distribution in the fin for various amounts of fin coverage with PCM. The thickness of the fin is 1 mm.

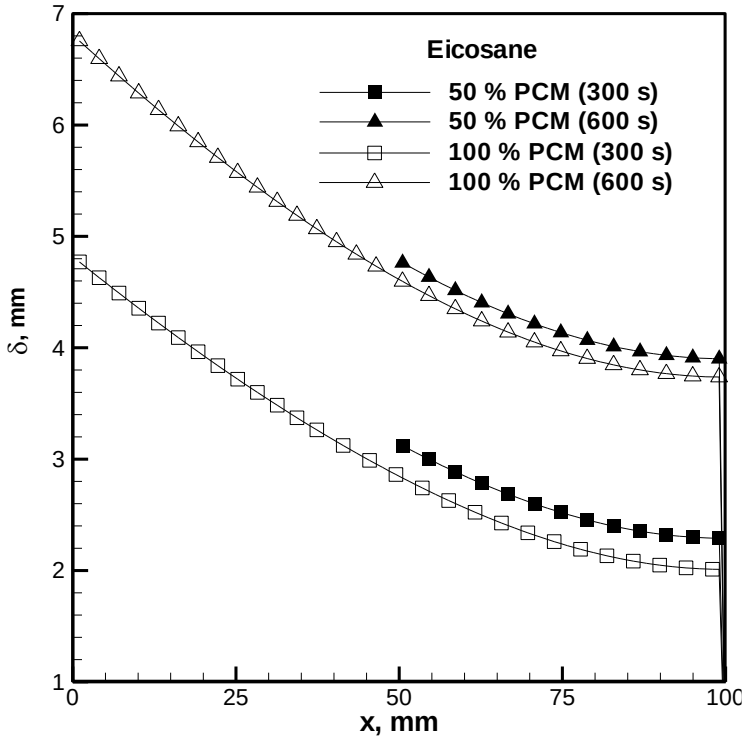

Figure 14: Spatial variation of melt depth for eicosane.

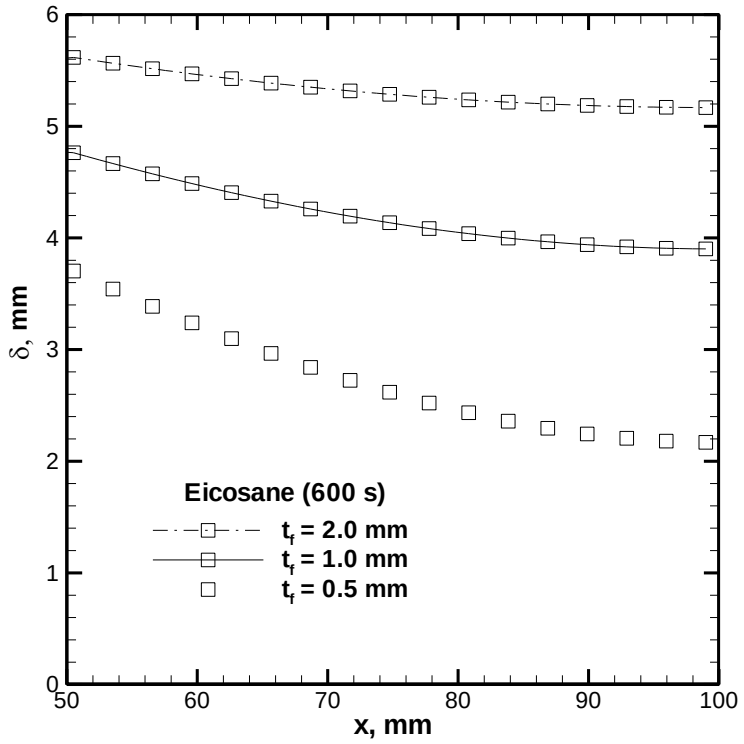

Figure 15: Melt depth for various thickness of the fin at 600 s.

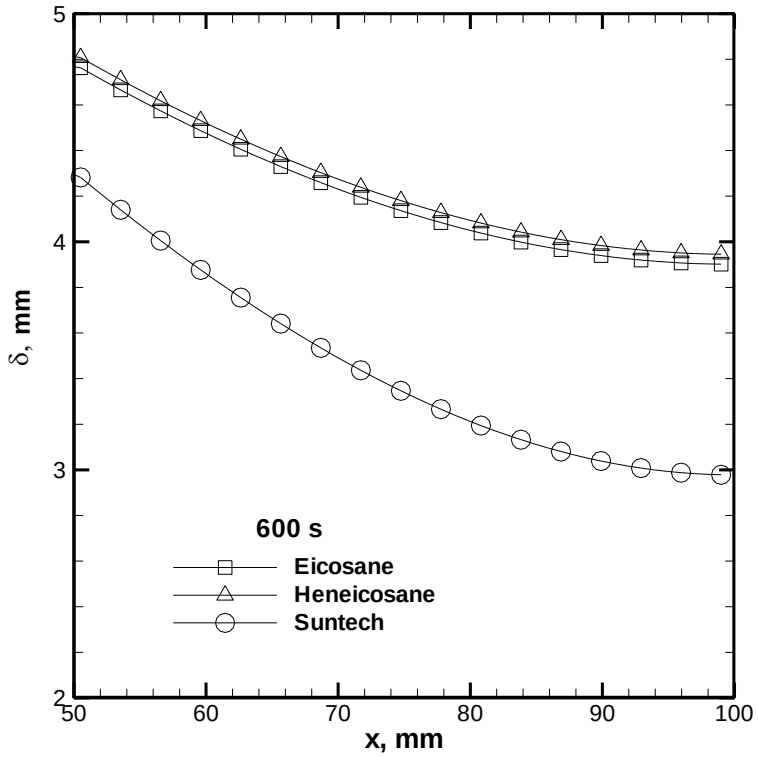

Figure 16: Melt depth variation for different PCMs considered.